Macromolecules

Article

Cite This: *Macromolecules* XXXX, XXX, XXX−XXX

Mechanisms of Directed Self-Assembly in Cylindrical Hole Confinements

Cody T. Bezik,[†] Grant P. Garner,[†] and Juan J. de Pablo*[,†,‡]

[†]Institute for Molecular Engineering, University of Chicago, Chicago, Illinois 60637, United States

[‡]Argonne National Laboratory, 9700 S Cass Ave., Argonne, Illinois 60439, United States

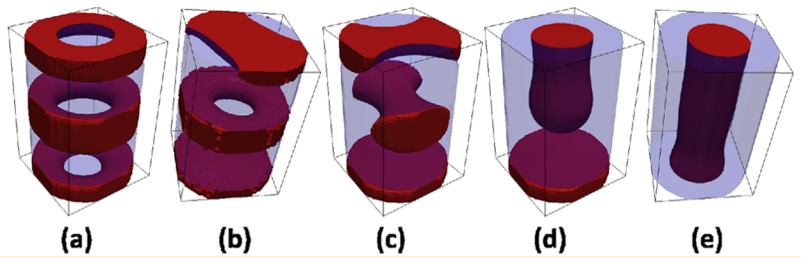

ABSTRACT: The directed self-assembly of block copolymers in cylindrical holes is a promising technology for lithographic patterning, particularly in the context of vertical interconnect accesses. While the hole-shrink process for single cylinders has been extensively explored, the proliferation of morphological defects remains a significant technological barrier. We use a coarse-grained model to explore morphologies that form within cylindrical confinements for combinations of template surface energies. We identify metastable defect morphologies, in addition to the desired cylindrical morphology, in majority-wetting sidewall templates. We use our coarse-grained model and the string method to identify transition pathways between defective morphologies and the cylindrical morphology to elucidate the mechanism of defect annihilation within the confinements; the transition pathway from a disordered state is also identified. This work demonstrates that the minimum free energy path for the formation of a cylinder goes through defective morphologies and that designing confinements can eliminate these undesirable transition states.

INTRODUCTION

As conventional optical lithographic techniques reach their resolution limit, and with many of the proposed replacements growing in cost, the directed self-assembly (DSA) of block copolymers has attracted considerable industrial interest as a means to achieve cost-efficient, high-resolution patterning at the nanoscale.[1−6] The DSA process relies on utilizing confinement design and chemically functionalized surfaces, referred to as graphoepitaxy[7−10] and chemoepitaxy,[11−15] respectively, in order to coerce a block copolymer morphology into a desired structure. These strategies have proven capable of yielding the assembly of lines[16] and cylinders[17] over large patterned areas.[18] Of particular interest for the fabrication of device-oriented structures is the assembly of cylindrical-phase block copolymers within cylindrical confinements (or "holes"), known as the hole-shrink process.[19] Such a process offers an inexpensive route toward efficient production of vertical interconnect accesses (VIAs) or cut masks.[20,21]

Cylindrical confinements have two unique surfaces: the sidewall of the holes and the circular bottom. The interfacial energy between each surface and each copolymer block needs to be carefully tuned, in concert with the template diameter, to induce the assembly of a desired cylinder. It has been demonstrated that cylinders can successfully form in smaller template diameters if the sidewall preference is for the majority block.[22,23] However, most theoretical work has focused on cylindrical templates where the sidewall surface is preferentially wet by the minority block of a cylinder-forming block copolymer.[24−27] Peters et al., using a theoretically informed coarse-grained model, demonstrated that increasing the affinity of the sidewall for the minority block leads to a stabilization of the desired through-film cylinder morphology over other metastable structures.[28] Laachi et al., utilizing a field-theoretic model, have also provided insights into the morphological, kinetic, and thermodynamic differences that exist between nonpreferential sidewalls and sidewalls that are preferentially wet by the minority block.[29] These studies collectively support the conclusion that a sidewall that is preferentially wet by the minority block provides a critical boundary condition for obtaining the desired cylindrical morphology. However, given that smaller template diameters have been found to stabilize well-ordered cylinders when the sidewall is preferentially wet by the majority block—a reduction from approximately twice the bulk domain spacing to a single bulk domain spacing—additional theoretical study is needed in order to understand assembly under such conditions.

Previous theoretical and simulation studies on such systems has confirmed the stability of a through-film cylinder at

Received: December 12, 2017
Revised: February 15, 2018

DOI: 10.1021/acs.macromol.7b02639
Macromolecules XXXX, XXX, XXX−XXX

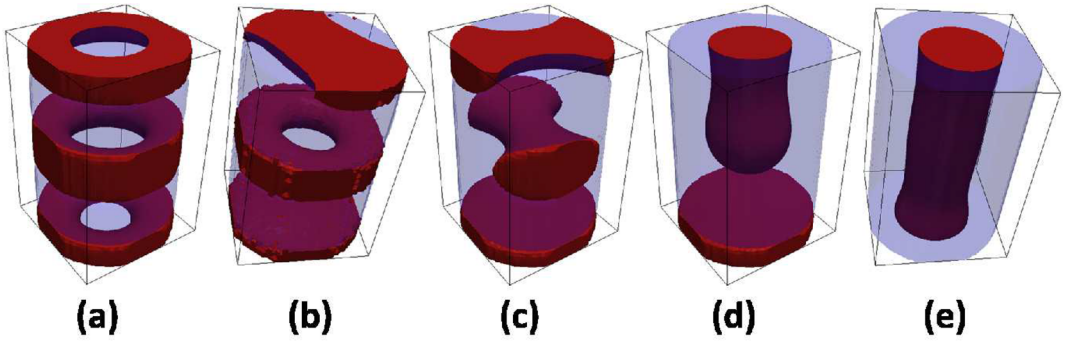

Figure 1. A compilation of the well-defined morphologies that were stabilized from independent Monte Carlo simulations of cylinder forming block copolymers. The dark, red phase represents the minority-block-rich domain, while the light blue phase is the majority-block-rich domain. The morphologies observed were (a) the double donut, 2D, (b) the donut bar, DB, (c) the double bar, 2B, (d) the disconnected cylinder, DC, and (e) the cylinder.

templates of approximately one bulk domain spacing in diameter,[30−33] though in general little attention has been paid to optimizing the strength of the sidewall attractiveness for the majority block to produce DSA relevant morphologies. There has also been extensive work on characterizing the phase diagram of block copolymers confined to cylindrical holes with respect to varying strength of sidewall interactions,[34] though at template dimensions larger than a single bulk domain spacing.

Recent experimental work by Doise et al. has shown that it is possible to experimentally control the wetting behavior of both the sidewalls and the bottom substrate independently through random block copolymer brushes.[35] This control has allowed for the modification of the wetting behavior of the sidewalls and bottom of the cylindrical confinements separately; furthermore, the random block copolymer brushes allowed for the surfaces to be preferential for either the majority block or the minority block. Through manipulation of the brush composition, these authors demonstrated the ability to use prepattern holes with smaller and larger critical dimensions (confinements with diameters of approximately 1 and 2 times the natural domain spacing, respectively) to drive the assembly of cylindrical morphologies. Doise et al. achieved successful assembly at an open hole rate greater than 95% in some cases (as verified via top-down SEM after pattern transfer); this relatively high threshold, however, does not meet the defectivity requirements for industrial applications, prompting further questions about how to optimize a prepattern to reduce or avoid defect formation in contact hole-shrink experiments.

The results reported by Doise et al. were generally in good agreement with predictions by Peters et al., but at the experimental level, confinement still led in some cases to defective assembly. The work of Peters et al. provided a qualitative understanding of which design rules are necessary for stabilizing a cylindrical morphology, but only considered the final—equilibrium—states reached in a simulation, without addressing how defective states form and remain stable or how transitions between defective states occur. Recent works by Li et al., Hur et al., and Laachi et al. have shown that a string method can be used in coarse-grained[36,37] and field-theoretic models,[25,29,38] respectively, to analyze transition pathways in block copolymer systems. These works provided an understanding of transitions between competitive structures in thin films and in cylindrical confinement but did not address how the formation of competitive, metastable states might interfere with morphology formation. In addition, in the context of exploring the transition between defective states and through-film cylinders in contact holes, the work of Laachi et al. only explored a limited number of prepattern configurations and did not consider how optimization of the prepattern might influence defectivity.

Here, we utilize a theoretically informed coarse-grained model for block copolymers, which has been shown to be in good agreement with experiment in past work, to explore the emergence of metastable states within cylindrical confinements with a critical dimension of approximately one domain spacing. Subsequently, we use the string method to analyze the transition between competitive states, uncovering the free energy barriers opposing the transition from metastable defects to through-film cylinders. The influence of the strength of the affinity of the sidewall and bottom substrates on these free energy barriers is also considered. Additionally, the transition from a disordered state to a through-film cylinder is investigated at varying template conditions.

We find that in a large sample of simulations repeated at the same set of conditions different final morphologies appear, including defects and through-film cylinders, indicating template conditions which stabilize various morphologies. Transition pathways calculated at prepattern conditions in the vicinity of these regions, where several different morphologies occur, reveal that significant free energy barriers exist that oppose the annihilation of defects, even if the defective states have a significantly higher free energy. The formation of these defects is associated with the fact that they are part of the most probable transition pathway from a disordered state to a through-film cylinder; that is, at certain conditions, a "direct" pathway from order to disorder is less favored than one in which defects occur.

RESULTS AND DISCUSSION

The cylindrical confinement for guiding the DSA process utilizes chemoepitaxy and graphoepitaxy to drive the assembly of cylindrical features that span the height of the confinement. The simulations in this work focus on perfectly cylindrical confinements that are filled with poly styrene-*b*-(methyl methacrylate), PS-*b*-PMMA, with a styrene volume fraction of $f_{PMMA} = 0.3$. The match between the simulated polymer and real PS-*b*-PMMA is provided by confirming that the simulated polymer reproduces the bulk periodicity of PS-*b*-PMMA; additionally, the chosen χN value is commensurate with PS-*b*-PMMA. We assume that the surfaces that produce the confinement, the vertical sidewall and the circular bottom, are unique in terms of their affinity for the polymer; thus, the block

DOI: 10.1021/acs.macromol.7b02639
Macromolecules XXXX, XXX, XXX−XXX

copolymer that is deposited inside the hole is assumed to have an independent interfacial energy with each surface. The strength of these interfacial energies is governed by the constants Λ_{SW} and Λ_B for the sidewall and bottom surfaces, respectively, and the surfaces interact with the polymer via the potential described below, where z is the distance between a polymer bead and the closest (normal) point on the given surface. A negative value indicates a preference for the minor block, poly(methyl methacrylate), PMMA, and a positive value indicates a preference for the major block, polystyrene, PS.

We performed a number of independent Monte Carlo simulations to investigate the impact of the combination of these parameters on a predicted morphology for constant confinement dimensions. A height of 62 nm, $1.67L_0$, and diameter of 43 nm, $1.16L_0$, were chosen in order to be in agreement with the experimental conditions used by Doise et al.[35] These values were well in the region of the design space that resulted in the desired cylindrical morphology (at least when viewed from a top down perspective, experimentally). Using this geometrical confinement, we set the interfacial energy constants to be $0.0 \leq \Lambda_{SW} \leq 1.0$ and $-1.0 \leq \Lambda_B \leq 0.0$. In this work, the sidewall is assumed to be preferential for PS (or neutral) and the bottom for PMMA (or neutral); again, this is in qualitative agreement with the experimental setup of Doise et al.[35] The simulations were run for 500 000 Monte Carlo sweeps to find the stable morphologies at each interfacial energy combination.

The results of these simulations revealed that five unique, well-defined morphologies were stable within this range of parametric combinations. A 3D rendering of those morphologies can be seen in Figure 1, which includes the double donut (2D), the donut bar (DB), the double bar (2B), the disconnected cylinder (DC), and the full cylinder (C). In some confinements, only one of these morphologies was stable across the set of simulations; however, there were many cases where more than one morphology was stable. This implies either that the states have comparable free energies or that the stabilized morphologies represent kinetically trapped metastable states. Figure 2 shows a diagram that illustrates which morphologies were stable at each parametric combination of interfacial energies. The interfacial energy combinations that stabilize multiple morphologies are denoted by the large beige circles surrounding the markers in Figure 2—these combinations are seen at the intersection of the areas of parameter space that stabilize only one structure. The points at these intersections have as potentially stable states the morphologies that are singularly stable in the adjacent areas of design space. Examples of these intersections exist at the combinations of (Λ_{SW},Λ_B) listed in Table 1. One of the interesting combinations of interfacial energies occurs around the "triple point", where the conditions that stabilize the double bar, the disconnected cylinder, and the cylinder morphologies coincide. At the values of $\Lambda_{SW} = 0.4$ and $\Lambda_B = -0.2$ the Monte Carlo simulations yield formation of all three of the aforementioned morphologies.

At this "triple point", where multiple possible stable states result arise in simulations, we can extract useful thermodynamic and kinetic information about their relative stability using the string method. We chose to analyze the transition pathway between a defective morphology and a cylinder beginning at the "triple point" ($\Lambda_{SW} = 0.4$ and $\Lambda_B = -0.2$) and then subsequently in its immediate vicinity in parameter space. This provided the opportunity to analyze the annihilation pathway

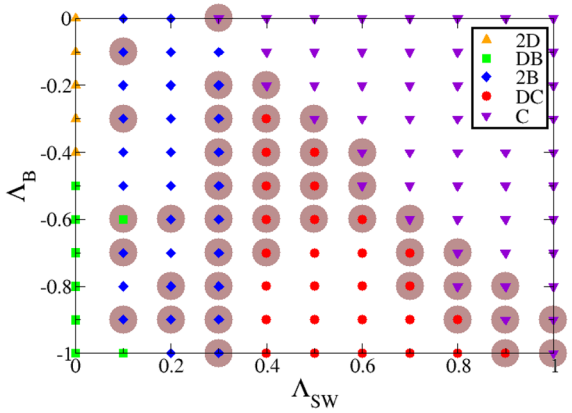

Figure 2. A phase diagram that shows which morphologies were most likely to form at a given combination of sidewall preference for the majority block, Λ_{SW}, and bottom preference for the minority block, Λ_B. Each combination of interfacial energies is given a marker that identifies which morphology was observed most often after 10 independent Monte Carlo simulations. The large beige circles denote interfacial energy combinations that resulted in multiple stable morphologies. The absence of a beige circle means that only one type of morphology was stabilized. The morphologies observed can be seen in Figure 1 and include the double donut (2D) denoted by orange upward pointing triangles, the donut bar (DB) denoted by green squares, the double bar (2B) denoted by blue diamonds, the disconnected cylinder (DC) denoted by the red circles, and the cylinder (C) denoted by the violet downward facing triangles.

Table 1. Stable Morphologies That Exist at Intersections in Design Space

Λ_{SW}	Λ_B	stable morphologies
0.1	−0.1	2B, 2D
0.1	−0.6	DB, 2B
0.4	−0.2	2B, C, DC
0.3	−0.6	2B, DC
0.6	−0.5	C, DC

for two different defects, the double bar, and the disconnected cylinder within a single confinement design.

First, we investigated the transition pathway between the double-bar and cylindrical morphologies using the string method. Figure 3 shows the MFEP calculated from the string between a double-bar structure ($\alpha = 0$) and the through-film cylinder ($\alpha = 1$) within a cylindrical confinement with $\Lambda_{SW} = 0.4$ and $\Lambda_B = -0.2$. Two clear transition states can be identified along this pathway. The first transition state is approximately $30k_BT$ higher in free energy compared to the metastable defect, and it corresponds to the formation of a PMMA bridge linking the upper and middle bars. For this bridge to form, a certain number of PMMA chains must diffuse through a layer of PS, a highly unfavorable and unlikely event—hence, the large barrier. Following the initial bridge formation, however, polymer can diffuse more easily through the bridge, corresponding to the downhill descent in free energy. The second transition state is approximately $15k_BT$ higher in free energy compared to the nearby metastable state, and it corresponds to the formation of a second PMMA bridge between the layer of polymer at the bottom and the growing PMMA structure in the middle. Just as was the case for the first bridge, the diffusion of the first few PMMA chains through the layer of PS is unfavorable, and so the free energy barrier is large. Once that process is initiated, however, there are no more free energy barriers, and polymer

DOI: 10.1021/acs.macromol.7b02639
Macromolecules XXXX, XXX, XXX−XXX

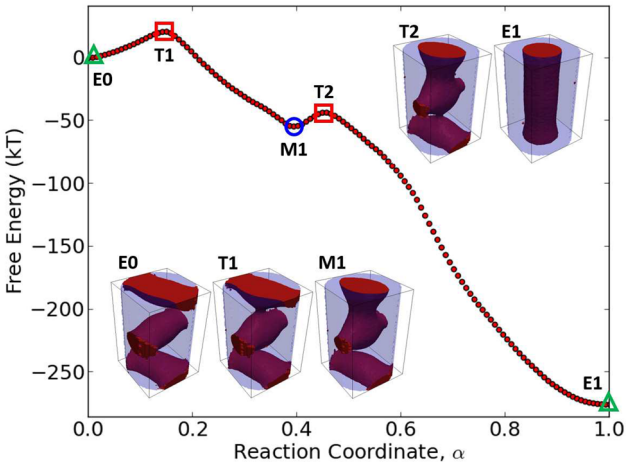

Figure 3. Transition pathway along the reaction coordinate α between a double bar morphology and a cylinder with $\Lambda_{SW} = 0.4$ and $\Lambda_B = -0.2$. The green triangles identify the end nodes of the string, the red squares identify the nodes of the string where the transition states occur, and the blue circles identify the location of the metastable states along the pathway. Graphics of the morphologies corresponding to the labeled nodes are included.

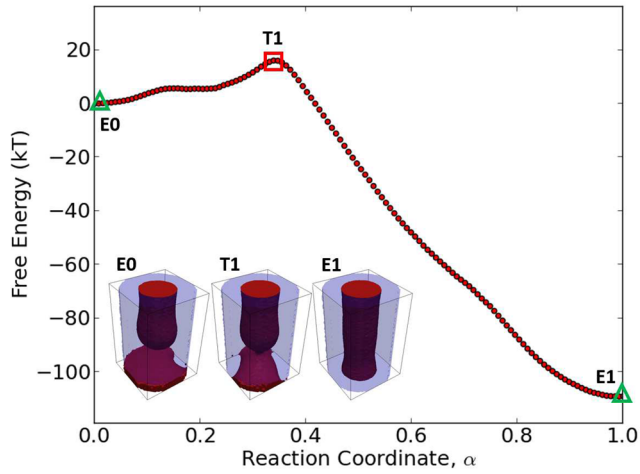

Figure 4. Transition pathway along the reaction coordinate α between a disconnected cylinder morphology and a cylinder with $\Lambda_{SW} = 0.4$ and $\Lambda_B = -0.2$. The green triangles identify the end nodes of the string, the red squares identify the nodes of the string where the transition states occur, and the blue circles identify the location of the metastable states along the pathway. Graphics of the morphologies corresponding to the labeled nodes are included.

simply diffuses through the established bridges to form a well-ordered, complete cylinder. We note the similarity in the connection of these domains to the merging of disconnected lamellae observed in previous studies of defect annihilation.[36,37,39]

It is of interest to consider why the opposite pathway is not favored—that is, the bottom bridge forming first, followed by the upper bridge. If the bottom bridge formation occurred first, it is expected that the first free energy barrier would be even higher because, in addition to requiring the same number of chains to diffuse the same distance, PS would be forced (due to the volume-filling nature of the model) to occupy space near the bottom substrate, a situation that is enthalpically unfavorable. This presumably large free energy barrier is circumvented when the system first forms the upper bridge; this also creates a bulge in the PMMA in the center of the system. Thus, when the bottom bridge does form, it need not traverse as great a distance, making up for the enthalpic penalty of forcing PS onto the bottom substrate. While this effect would likely be observed in the opposite pathway as well, it is the avoidance of the first very large barrier that is expected to be most critical.

Next, we fixed the end states of the string to be the disconnected cylinder and the complete cylinder morphologies. The calculated MFEP for the annihilation of this defective morphology can be seen in Figure 4. The MFEP for annihilation of the disconnected cylinder is similar to the last half of the annihilation of the double-bar, including a transition state that is approximately $20k_BT$ higher than the metastable defect. Likewise, this free energy barrier corresponds to the formation of a PMMA bridge between the bottom layer and the disconnected cylinder, requiring the unfavorable diffusion of PMMA through a PS layer. Indeed, it can be observed in Figure 3 that a metastable morphology very much like that corresponding to the disconnected cylinder exists in the middle of the pathway.

It is now clear that these defective morphologies are not competitive at equilibrium but instead represent long-lived kinetically trapped states. Despite the fact that a confinement design can be conceived to thermodynamically favor formation of a complete cylinder, there can simultaneously exist significant barriers that must be overcome if the assembly process initially leads to an undesirable, metastable structure. In an attempt to understand how design parameters affect these barriers, we performed string calculations for several interfacial energy combinations.

Figure 5 shows the effect that the sidewall interfacial energy has on the transition barriers by varying the value of Λ_{SW} = {0.3, 0.4, 0.5} while $\Lambda_B = -0.2$. There is a significant reduction in the free energy barriers associated with both transition states as the sidewall becomes more preferential for the majority block, PS. Meanwhile, the free energy barriers grow much larger if the interaction parameter on the sidewall becomes more weakly preferential for PS.

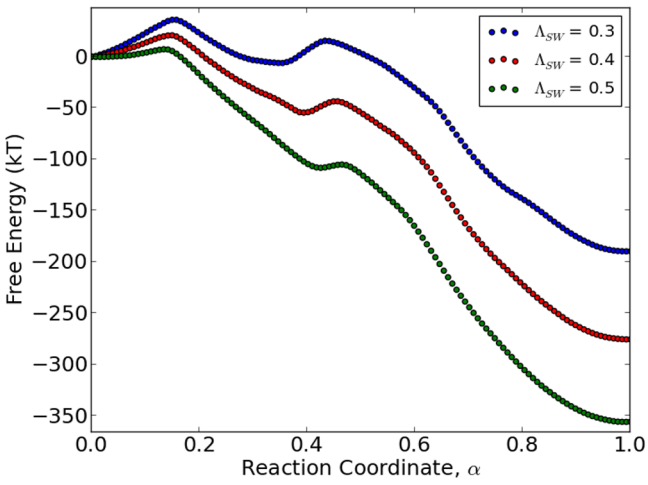

Figure 5. Three transition pathway along the reaction coordinate α between a double bar morphology and a cylinder with $\Lambda_B = -0.2$ where the sidewall interfacial energy is varied between Λ_{SW} = {0.3, 0.4, 0.5}.

DOI: 10.1021/acs.macromol.7b02639
Macromolecules XXXX, XXX, XXX−XXX

Figure 6 also shows how the MFEP changes when the interfacial energy corresponding to the interaction between the bottom of the confinement and the polymer changes if we use $\Lambda_B = \{-0.1,-0.2,-0.3\}$ while $\Lambda_{SW} = 0.4$. In contrast to the sidewall interfacial energy, the bottom of the confinement has only a small effect on the barrier heights of the transition states. The first transition is virtually unaffected, and there is a minor influence on the height of the second free energy barrier. As discussed previously, part of the barrier associated with this latter transition is the forcing of PS to the bottom substrate as PMMA diffuses to the center. If the bottom substrate is less hostile to PS, there is less of a penalty associated with this transition. Furthermore, this observation also explains the reduction in the thermodynamic free energy difference between the two-bar structure and the full cylinder. The volume of PS wetting the bottom surface is greater in the full cylinder morphology than the two-bar morphology; increasing the preference for PMMA of the bottom surface therefore causes a greater perturbation to the free energy of the full cylinder morphology, resulting in the reduction in thermodynamic preference.

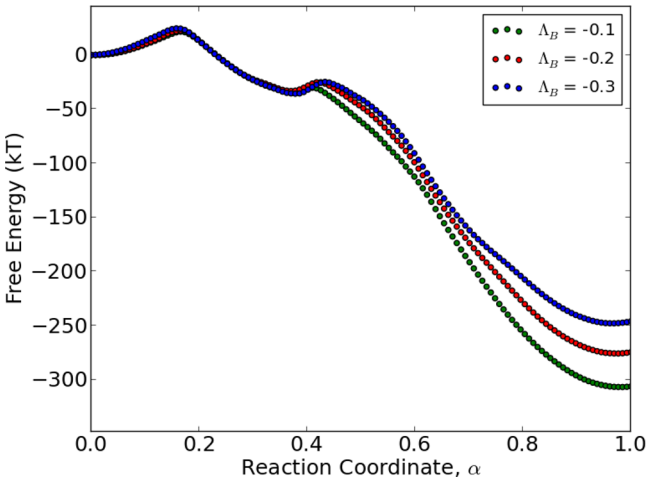

Figure 6. Three transition pathway along the reaction coordinate α between a double bar morphology and a cylinder with $\Lambda_{SW} = 0.4$ where the bottom interfacial energy is varied between $\Lambda_B = \{-0.1, -0.2, -0.3\}$.

The simulation results in Figures 5 and 6 show that the two unique surfaces comprising the guiding confinement have different effects on the thermodynamics and kinetics of the hole-shrink process. These results indicate that it is more important to control the sidewall surface characteristics when trying to minimize the kinetic barriers that exist between defective states such as the two-bar structure and the desired full cylinder morphology. This follows intuition, as the full cylinder morphology needs the majority phase to wet the entirety of the sidewalls of the confinement for the cylinder to exist.

The previous discussion helps us understand why, for a given set of conditions, defective morphologies such as the double-bar or disconnected cylinder structures might persist in a cylindrical confinement; however, it does not completely clarify why such structures may appear in the first place, especially given the thermodynamic free energy difference between the defective structure and the through-film cylinder. To address this issue, a series of strings were calculated that connect a disordered state and a through-film cylinder in confinements having varying sidewall energy strengths; the resulting MFEPs are shown in Figures 7, 8, and 9. The disordered states were produced by performing Monte Carlo simulations of a block copolymer with identical parameters to the polymer used for all other calculations in this work, except with $\chi N = 0.0$. This

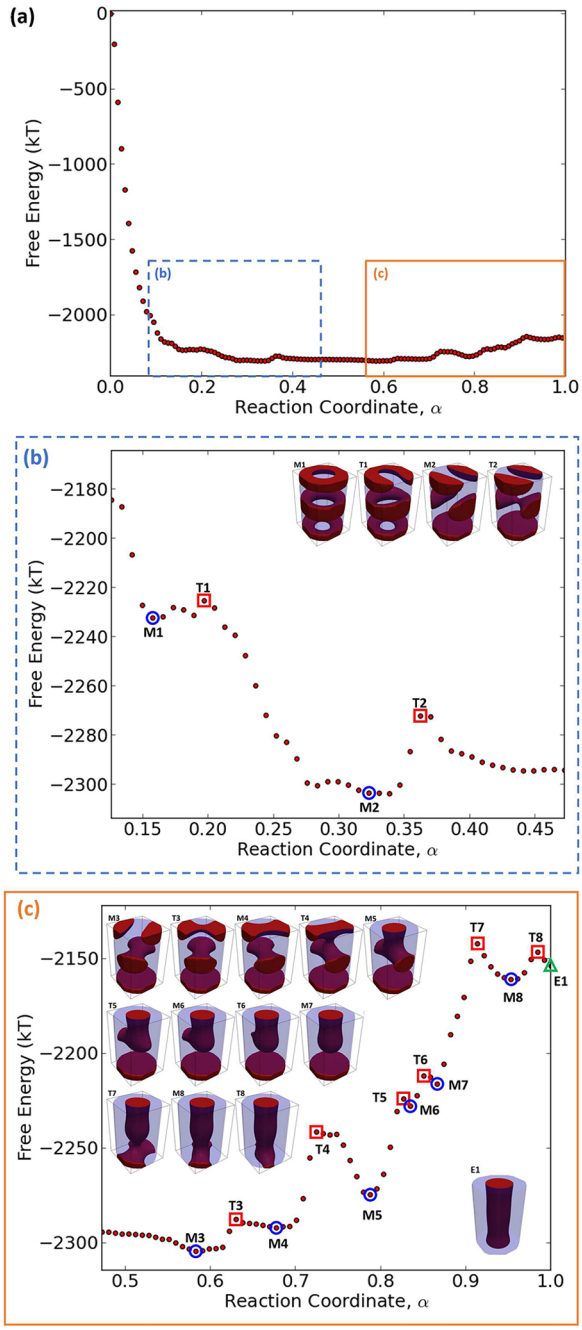

Figure 7. Transition pathway along the reaction coordinate α between a disordered block copolymer and a cylinder with $\Lambda_{SW} = 0.0$ and $\Lambda_B = -0.2$. (b) and (c) are zoomed-in segments of the pathway that are included to visualize the features of the calculated minimum free energy pathway. The green triangle identifies the end node of the string that corresponds to the cylindrical morphology, the red squares identify the nodes of the string where the transition states occur, and the blue circles identify the location of the metastable states along the pathway. Graphics of the morphologies corresponding to the labeled nodes are included.

DOI: 10.1021/acs.macromol.7b02639
Macromolecules XXXX, XXX, XXX−XXX

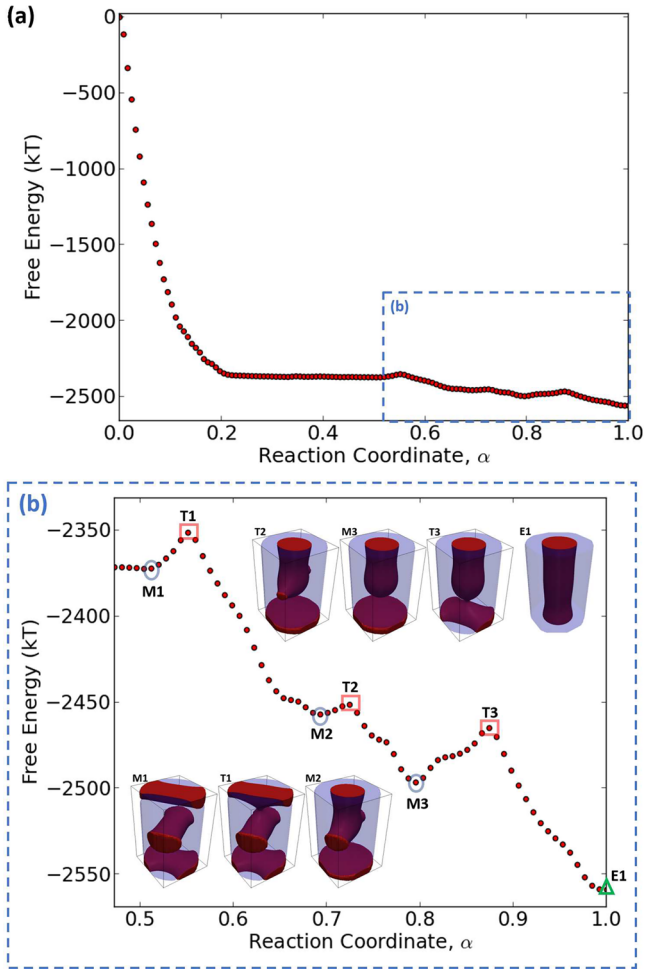

Figure 8. Transition pathway along the reaction coordinate α between a disordered block copolymer and a cylinder with $\Lambda_{SW} = 0.3$ and $\Lambda_B = -0.2$. (b) is a zoomed-in segment of the pathway that is included to visualize the features of the calculated minimum free energy pathway. The green triangle identifies the end node of the string that corresponds to the cylindrical morphology, the red squares identify the nodes of the string where the transition states occur, and the blue circles identify the location of the metastable states along the pathway. Graphics of the morphologies corresponding to the labeled nodes are included.

provided a realistic configuration corresponding to a disordered state, as the MC simulation allowed bond lengths to equilibrate, while the lack of any driving force for segregation between the polymers allowed them to mix freely.

Unsurprisingly, the free energy difference between the disordered state and the through-film cylinders is large, on the order of $2000k_BT$, regardless of sidewall wetting behavior (these differences do grow larger as the sidewall preference grows stronger for PS). However, the MFEP for the neutral sidewall ($\Lambda_{SW} = 0.0$), shown in Figure 7, has eight distinct transition states, labeled by the red squares along the plotted transition pathway, with barriers on the order of $10k_BT$. Each of these transition states can be linked to a diffusion event that results in a compression of an existing minority-rich domain, as seen in T1, T5, T6, and T8, or the bridging of two nearby minority-rich domains, as seen in T2, T3, T4, and T7. The relative magnitudes of the energy barriers associated with these two types of phenomena show that the diffusion events that bridge two domains require more energy. This can be explained

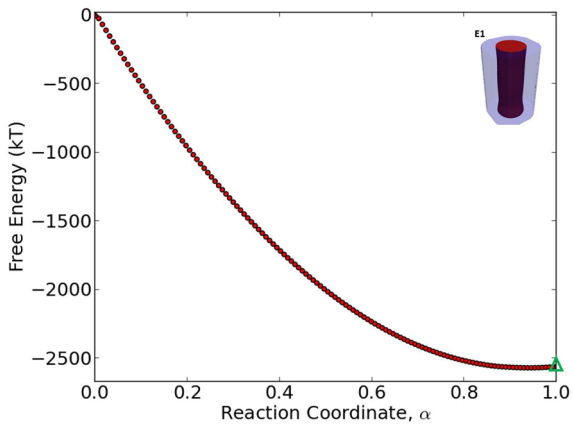

Figure 9. Transition pathway along the reaction coordinate α between a disordered block copolymer and a cylinder with $\Lambda_{SW} = 0.5$ and $\Lambda_B = -0.2$. There is no zoomed-in segment of the pathway included as the calculated minimum free energy pathway is absent of other metastable sates. The green triangle identifies the end node of the string that corresponds to the cylindrical morphology. A graphic of the cylindrical morphology corresponding to the labeled node is included.

by the increase in interfacial area resulting from the bridging event and the reduction of interfacial area of a compression event. A larger interfacial area simultaneously increases the entropy and enthalpy of the system, resulting in a considerable activation barrier for the event. These large barriers, along with the fact that a number of the metastable states along this path are lower in free energy than the desired cylinder structure, provide insights into the difficulty of assembling cylinders within confinements that are not preferentially wet by the majority block.

At a greater sidewall preference for the majority block ($\Lambda_{SW} = 0.3$) the transition states such as the donut morphologies disappear from the MFEP toward a cylinder structure, as shown in Figure 8. This increased preference for the majority block also stabilizes the desired morphology relative to the other metastable states, making the cylinder the lowest energy structure along the pathway. However, there still exist multiple barriers—on the order of $10k_BT$—that must be overcome to assemble the cylinder.

These barriers and transition states can be completely eliminated from the transition pathway to a cylinder by further increasing the interfacial energy of the sidewall, as shown in Figure 9 where $\Lambda_{SW} = 0.5$. In fact, for this more strongly preferential sidewall, the path from disorder to a cylindrical structure proceeds downhill for the entirety of the formation of a cylinder, with no transition states or metastable states along the way.

This provides evidence that if a sidewall surface can be designed that exhibits a sufficiently strong preference for the majority block, then the MFEP toward the desired cylindrical morphology is void of unwanted metastable morphologies. It is likely that continuing to increase the sidewall preference for the majority block will improve dynamics of assembly as well as the thermodynamics. It is our belief that many pathways, including those that pass through defects and those which do not, remain competitive regardless of which is most probable. Therefore, continued increase of the sidewall preference for the majority block is likely to give rise to defect-free pathways progressively less probable. Quantifying this effect is a future direction of interest.

DOI: 10.1021/acs.macromol.7b02639
Macromolecules XXXX, XXX, XXX−XXX

Furthermore, we acknowledge that increasing the wetting behavior within a simulation is different than what can be done in experimental systems. While there are kinetic and thermodynamic benefits to using highly preferential sidewalls for the majority block, there is no guarantee that an experimental confinement can be designed to be selective enough to realize the elimination of metastable states along the most probable path for cylinder formation. Lastly, we acknowledge that experimental assembly may not begin entirely from disorder; assembly may already have begun at an earlier stage of an experimental assembly process.

CONCLUSIONS

The systematic study of the single-hole shrink process where the sidewalls are wet by the majority block of a cylinder forming block copolymer has allowed for the identification of the metastable states that may arise depending on confinement design. Subsequent application of the string method has enabled a detailed analysis of the transition pathways between defective states and the desirable through-film cylindrical morphology—specifically, the study of a single design chemistry where three different morphologies were stabilized in independent Monte Carlo simulations: a double-bar, a disconnected cylinder, and a complete cylinder. The complete cylinder was identified to be the morphology with the lowest free energy of the three; however, the transition pathway between the desired morphology and the defects was found to exhibit significant energetic barriers of approximately $30k_BT$. This finding provides insights into the challenges associated with reaching industrial defect standards, as the diffusion events necessary to transition from a defect to a cylinder are unlikely to occur if the system ends up in a defective state. Altering the sidewall chemistry has been shown to have a much more significant impact on these pathways than the chemistry of the bottom surface. To complete the understanding of defectivity, we demonstrated a method to identify the most likely transition pathway for forming a cylinder from a disordered melt. In confinements with low preference for the majority block, the minimum free energy path for forming a cylinder goes through numerous metastable states separated by large barriers. We demonstrated that this MFEP is fundamentally changed in confinements with preferential sidewalls. As the sidewall becomes more preferential for the majority block, the number of metastable states that exist in the pathway is reduced until, for a sufficiently strong preference, the MFEP proceeds downhill, going straight to the desired cylindrical morphology. We note that the string method used to find this pathway is only able to identify a single, most probable transition path and does not speak to the relative probability of proceeding down this path. However, the demonstrated ability to fundamentally change the most probable path using confinement design is promising, as it implies that if the sidewalls of these confinements can be created to be highly preferential for the majority block, the resulting hole-shrink process will be better suited to meet industrial defect standards.

METHODS

The simulation results presented in this work are based on the standard theoretically informed coarse-grained model,[40−42] which represents n block copolymer Gaussian chains discretized into N beads connected by harmonic springs in a fixed volume V at a fixed temperature T. This model has previously been shown to be in quantitative with experimental results.[43,44] In this model, the energy associated with the polymer bonds is expressed as

$$\frac{H_b[\{\mathbf{r}_i(s)\}]}{k_BT} = \frac{3}{2b^2}\sum_{i=1}^{n}\sum_{s=1}^{N-1}[\mathbf{r}_i(s+1) - \mathbf{r}_i(s)]^2 \quad (1)$$

where the sth bead on the ith chain has position $\mathbf{r}_i(s)$. R_e is the end-to-end distance of the polymer chains; typically, a unit system is adopted for the simulations where the end-to-end distance is unity. Additionally, k_B is the Boltzmann constant. The energy associated with nonbonded interactions is given as

$$\frac{H_{nb}[\phi_A, \phi_B]}{k_BT} = \frac{\sqrt{\bar{N}}}{R_e^3}\int_V d\mathbf{r}\left[\chi_{AB}N\phi_A\phi_B + \frac{\kappa N}{2}(1 - \phi_A - \phi_B)^2\right] \quad (2)$$

where $\sqrt{\bar{N}} = \frac{\rho_0 R_e^3}{N}$, the interdigitation number, is an estimate of the number of chains a given chains interacts with (ρ_0 is the average bulk number density of beads). The parameter χN is the Flory−Huggins parameter governing the incompatibility of the two blocks, and κ^{-1} is proportional to the melt compressibility. Each term $\phi(r)$ is a function of the local density of each type of bead; these densities are calculated by a particle-to-mesh (PM_0) scheme, where the underlying grid is composed of cubic cells with side length ΔL.

The cylindrical confinement is imposed by hard walls; the sidewall and bottom substrate interact with the polymer according to

$$\frac{H_S}{k_BT} = \sum_{i=1}^{nN} f_s(x, y, K)\frac{\Lambda^K}{Nd_s}\exp\left(\frac{-z^2}{2d_s^2}\right) \quad (3)$$

where K is the type of monomer bead; the term $f_s(x,y,K)$ adopts a value of either -1 or 1, depending on the value of K and the position of the bead. Λ^K defines the strength of interaction between the surface and the bead; when a bead of type A is in a position preferable to type B, the overall energy contribution should be positive, and $\Lambda^A = -\Lambda^B$. Lastly, z is the distance to the surface, and d_s is the decay length of the potential. Both the sidewall and the bottom surface contribute a term of this form. The model is implemented in the context of a Monte Carlo simulation. Configurations are sampled according to the Metropolis criterion, where the probability of accepting a trial configuration is given by $p_{acc} = \exp(-\Delta H/(k_BT))$. Trial configurations are proposed using two different Monte Carlo moves: single bead displacement and chain reptation.

To find the minimum free energy pathways between two states of interest, we make use of the string method as described by Maragliano et al.[36,45−54] A string of points is constructed to connect two end states; each point along the string, or image, represents a unique morphology. The string is mathematically described as $\mathbf{m}(\alpha)$ where α is the reaction coordinate ($0 \le \alpha \le 1$). The images are vectors, each component m_i of which is a function of an order parameter constructed from the local densities on a grid. At each point r_i in the grid, $m_i = \frac{\phi_A(r_i) - \phi_B(r_i)}{\phi_A(r_i) + \phi_B(r_i)}$. This quantity represents the normalized density differences between beads of type A and B in a volume ΔL^3 around each point r_i in a grid that spans the entire simulation box.

The condition for the string to be the MFEP is that the perpendicular component of the gradient of the mean force

DOI: 10.1021/acs.macromol.7b02639
Macromolecules XXXX, XXX, XXX−XXX

along the string must be zero everywhere. The potential of mean force on the string, defined at each image, is given by

$$F(\mathbf{m}) = -k_B T \ln \int \mathrm{d}\{\mathbf{r}^{nN}\} \exp\left(-\frac{H}{k_B T}\right)\delta[\mathbf{m} - \hat{\mathbf{m}}] \quad (4)$$

In this equation, $\hat{\mathbf{m}}$ indicates the order parameter vector constructed from the particle coordinates $\{\mathbf{r}^{nN}\}$. The MFEP satisfies $\nabla_\perp F(\mathbf{m}) = 0$, which means that the variation perpendicular to the path is zero everywhere along the path. The mean force is numerically calculated via umbrella sampling with a harmonic restraint; the total Hamiltonian has the additional term

$$\frac{H_c}{k_B T} = \frac{\lambda}{2}\int_V \mathrm{d}\mathbf{r}[\mathbf{m} - \hat{\mathbf{m}}]^2 \quad (5)$$

where λ is a spring constant that controls the strength of the restraining potential. In the limit of an infinitely large spring constant, the free energy of the restrained system converges to the free energy functional $F(\mathbf{m})$. Using a spatial grid to evaluate the integral in the umbrella potential, the differential of free energy with respect to $\mathbf{m}$ goes to $\frac{\delta F}{\delta \mathbf{m}} = \lambda \Delta L^3 k_B T[\mathbf{m} - \langle\hat{\mathbf{m}}\rangle_c]$, where $\langle\hat{\mathbf{m}}\rangle$ is averaged over many MC steps. Therefore, the string is updated every iteration according to $\mathbf{m}_{k+1} = \mathbf{m}_k - \tau\lambda\Delta L^3[\mathbf{m}_k - \langle\hat{\mathbf{m}}\rangle_c]$, where τ is a time constant controlling the frequency at which the string is updated. As described in Maragliano et al., the images are redistributed after every iteration to keep them from falling into the minima of the free energy landscape.[49]

In our work the string is discretized into 128 nodes, each of which is an independent MC simulation used to estimate the mean force along the string. Note that preliminary calculations showed that 64 images are insufficient, and more than 128 images do not change the final pathway appreciably. The free energy along the string can be determined from the free energy estimation method outlined in Maragliano et al.[49] The strings were initialized as linear interpolations in collective variable space between a defective morphology (or a disordered melt), $\alpha = 0$, and a perfect, through-film cylinder, $\alpha = 1$. These states were chosen from independent MC simulations. When calculating pathways between defects and ordered cylinders, the ends of the string are free to move, ensuring the ends represent local minima. When calculating pathways between disorder and ordered cylinders, the first string node is fixed, while the others move in accordance with the string method (in anticipation that the disordered state will not represent a local free energy minimum, but instead an unstable state).

AUTHOR INFORMATION

Corresponding Author

*E-mail depablo@uchicago.edu; Tel 773-702-7791 (J.J.d.P.).

ORCID

Cody T. Bezik: 0000-0002-1940-4895

Juan J. de Pablo: 0000-0002-3526-516X

Author Contributions

C.T.B. and G.P.G contributed equally to this work.

Notes

The authors declare no competing financial interest.

ACKNOWLEDGMENTS

The study of assembly pathways and the development of the TICG model used here to describe copolymers were supported by the Department of Energy (DOE), Office of Science, Basic Energy Sciences (BES), Materials Science and Engineering (MSE) Division. The development of codes for advanced sampling simulations, including finite-temperature string simulations, was also supported by the D.O.E. through the MiCCoM center. The development of processes for defect-free assembly of copolymers for applications in next-generation lithography was supported by the U.S. Department of Commerce, National Institute of Standards and Technology, as part of the Center for Hierarchical Materials Design (CHiMaD) − 70NHNB14H012.

REFERENCES

(1) Jeong, S.-J.; Kim, J. E.; Moon, H.-S.; Kim, B. H.; Kim, S. M.; Kim, J. B.; Kim, S. O. Soft Graphoepitaxy of Block Copolymer Assembly with Disposable Photoresist Confinement. *Nano Lett.* **2009**, *9*, 2300−2305.

(2) Cheng, J. Y.; Mayes, A. M.; Ross, C. A. Nanostructure engineering by templated self-assembly of block copolymers. *Nat. Mater.* **2004**, *3*, 823−828.

(3) Cheng, J. Y.; Sanders, D. P.; Truong, H. D.; Harrer, S.; Friz, A.; Holmes, S.; Colburn, M.; Hinsberg, W. D. Simple and versatile methods to integrate directed self-assembly with optical lithography using a polarity-switched photoresist. *ACS Nano* **2010**, *4*, 4815−4823.

(4) Kato, H.; Seino, Y.; Yonemitsu, H.; Sato, H.; Kanno, M.; Kobayashi, K.; Kawanishi, A.; Imamura, T.; Omura, M.; Nakamura, N.; Azuma, T. Sub-30nm via interconnects fabricated using directed self-assembly. *Microelectron. Eng.* **2013**, *110*, 152−155.

(5) Seino, Y.; Yonemitsu, H.; Sato, H.; Kanno, M.; Kato, H.; Kobayashi, K.; Kawanishi, A.; Azuma, T.; Muramatsu, M.; Nagahara, S.; Kitano, T.; Toshima, T. Contact hole shrink process using directed self-assembly. *Proc. SPIE* **2012**, 83230Y−83230Y-7.

(6) Ma, Y.; Torres, J. A.; Fenger, G.; Granik, Y.; Ryckaert, J.; Vanderberghe, G.; Bekaert, J.; Word, J. Challenges and opportunities in applying grapho-epitaxy DSA lithography to metal cut and contact/via applications. *Proc. SPIE* **2014**, 92310T.

(7) Segalman, R. A.; Yokoyama, H.; Kramer, E. Graphoepitaxy of Spherical Domain Block Copolymer Films. *Adv. Mater.* **2001**, *13*, 1152−1155.

(8) Segalman, R. A.; Hexemer, A.; Kramer, E. J. Effects of Lateral Confinement on Order in Spherical Domain Block Copolymer Thin Films. *Macromolecules* **2003**, *36*, 6831−6839.

(9) Segalman, R. A.; Schaefer, K. E.; Fredrickson, G. H.; Kramer, E. J.; Magonov, S. Topographic Templating of Islands and Holes in Highly Asymmetric Block Copolymer Films. *Macromolecules* **2003**, *36*, 4498−4506.

(10) Segalman, R. A.; Hexemer, A.; Kramer, E. J. Edge Effects on the Order and Freezing of a 2D Array of Block Copolymer Spheres. *Phys. Rev. Lett.* **2003**, *91*, 196101.

(11) Stoykovich, M. P.; Muller, M.; Kim, S. O.; Solak, H. H.; Edwards, E. W.; de Pablo, J. J.; Nealey, P. F. Directed assembly of block copolymer blends into nonregular device-oriented structures. *Science* **2005**, *308*, 1442−1446.

(12) Stoykovich, M. P.; Kang, H.; Daoulas, K. C.; Liu, G.; Liu, C.-C.; de Pablo, J. J.; Muller, M.; Nealey, P. F. Directed Self-Assembly of Block Copolymers for Nanolithography: Fabrication of Isolated Features and Essential Integrated Circuit Geometries. *ACS Nano* **2007**, *1*, 168−175.

(13) Kim, S. O.; Solak, H. H.; Stoykovich, M. P.; Ferrier, N. J.; De Pablo, J. J.; Nealey, P. F. Epitaxial self-assembly of block copolymers on lithographically defined nanopatterned substrates. *Nature* **2003**, *424*, 411−414.

(14) Ruiz, R.; Kang, H.; Detcheverry, F. A.; Dobisz, E.; Kercher, D. S.; Albrecht, T. R.; de Pablo, J. J.; Nealey, P. F. Density Multiplication

DOI: 10.1021/acs.macromol.7b02639
Macromolecules XXXX, XXX, XXX−XXX

and Improved Lithography by Directed Block Copolymer Assembly. *Science* **2008**, *321*, 936−939.
(15) Liu, G.; Ramírez-Hernández, A.; Yoshida, H.; Nygård, K.; Satapathy, D. K.; Bunk, O.; de Pablo, J. J.; Nealey, P. F. Morphology of Lamellae-Forming Block Copolymer Films between Two Orthogonal Chemically Nanopatterned Striped Surfaces. *Phys. Rev. Lett.* **2012**, *108*, 065502.
(16) Cheng, J. K.; Rettner, C. T.; Sanders, D. P.; Kim, H. C.; Hinsberg, W. D. Dense self-assembly on sparse chemical patterns: Rectifying and multiplying lithographic patterns using block copolymers. *Adv. Mater.* **2008**, *20*, 3155−3158.
(17) Park, C.; Cheng, J. Y.; Fasolka, M. J.; Mayes, A. M.; Ross, C. A.; Thomas, E. L.; De Rosa, C. Double textured cylindrical block copolymer domains via directional solidification on a topographically patterned substrate. *Appl. Phys. Lett.* **2001**, *79*, 848−850.
(18) Park, S. M.; Stoykovich, M. P.; Ruiz, R.; Zhang, Y.; Black, C. T.; Nealey, P. F. Directed Assembly of Lamellae Forming Block Copolymers by Using Chemically and Topographically Patterned Substrates. *Adv. Mater.* **2007**, *19*, 607−611.
(19) Younkin, T. R.; Gronheid, R.; Delgadillo, P. A. R.; Chan, B. T.; Vandenbroeck, N.; Demuynck, S.; Romo-Negreira, A.; Parnell, D.; Nafus, K.; Tahara, S.; Somervell, M. Progress in directed self-assembly hole shrink applications. *Proc. SPIE* **2013**, 86820L.
(20) Tiron, R.; Gharbi, A.; Argoud, M.; Chevalier, X.; Belledent, J.; Pimmenta Barros, P.; Navarro, C.; Cunge, G.; Barnola, S.; Pain, L.; Asai, M.; Pieczulewski, C. The potential of block copolymer's directed self-assembly for contact hole shrink and contact multiplication. *Proc. SPIE* **2013**, *8680*, 868012−868012−11.
(21) Torres, J. A.; Sakajiri, K.; Fryer, D.; Granik, Y.; Ma, Y.; Krasnova, P.; Fenger, G.; Nagahara, S.; Kawakami, S.; Rathsack, B.; Khaira, G.; de Pablo, J.; Ryckaert, J. Physical verification and manufacturing of contact/via layers using grapho-epitaxy DSA processes. *Proc. SPIE* **2014**, *9053*, 90530R.
(22) Tiron, R.; et al. Template affinity role in CH shrink by DSA planarization. *Proc. SPIE* **2015**, 942317.
(23) Gronheid, R.; Doise, J.; Bekaert, J.; Chan, B. T.; Karageorgos, I.; Ryckaert, J.; Vandenberghe, G.; Cao, Y.; Lin, G.; Somervell, M.; Fenger, G.; Fuchimoto, D. Implementation of templated DSA for via layer patterning at the 7nm node. *Proc. SPIE* **2015**, 942305.
(24) Iwama, T.; Laachi, N.; Delaney, K. T.; Kim, B.; Fredrickson, G. H. Computational studies of shape rectification in directed self-assembly. *Proc. SPIE* **2014**, 904927.
(25) Iwama, T.; Laachi, N.; Delaney, K. T.; Fredrickson, G. H. Field-theoretic Simulations of Directed Self-assembly for Contact Multiplication. *J. Photopolym. Sci. Technol.* **2015**, *28*, 689−693.
(26) Latypov, A.; Preil, M.; Schmid, G.; Xu, J.; Yi, H.; Yoshimoto, K.; Zou, Y. *Exploration of the directed self-assembly based nano-fabrication design space using computational simulations*; Alternative Lithographic Technologies V., 2013; p 868013.
(27) Yoshida, A.; Yoshimoto, K.; Ohshima, M. Effect of wall potential on morphology of symmetric diblock copolymers in nanotrench. *Jpn. J. Appl. Phys.* **2016**, *55*, 06GE01.
(28) Peters, B. L.; Rathsack, B.; Somervell, M.; Nakano, T.; Schmid, G.; De Pablo, J. J. Graphoepitaxial assembly of cylinder forming block copolymers in cylindrical holes. *J. Polym. Sci., Part B: Polym. Phys.* **2015**, *53*, 430−441.
(29) Laachi, N.; Delaney, K. T.; Kim, B.; Hur, S.-M.; Bristol, R.; Shykind, D.; Weinheimer, C. J.; Fredrickson, G. H. Self-consistent field theory investigation of directed self-assembly in cylindrical confinement. *J. Polym. Sci., Part B: Polym. Phys.* **2015**, *53*, 142−153.
(30) Yu, B.; Sun, P.; Chen, T.; Jin, Q.; Ding, D.; Li, B.; Shi, A.-C. Confinement-Induced Novel Morphologies of Block Copolymers. *Phys. Rev. Lett.* **2006**, *96*, 138306.
(31) Li, W.; Wickham, R. A. Self-Assembled Morphologies of a Diblock Copolymer Melt Confined in a Cylindrical Nanopore. *Macromolecules* **2006**, *39*, 8492−8498.
(32) Li, W.; Wickham, R. A. Influence of the Surface Field on the Self-Assembly of a Diblock Copolymer Melt Confined in a Cylindrical Nanopore. *Macromolecules* **2009**, *42*, 7530−7536.
(33) Liu, M.; Li, W.; Wang, X. Order-order transitions of diblock copolymer melts under cylindrical confinement. *J. Chem. Phys.* **2017**, *147*, 114903.
(34) Li, W.; Wickham, R. A.; Garbary, R. A. Phase Diagram for a Diblock Copolymer Melt under Cylindrical Confinement. *Macromolecules* **2006**, *39*, 806−811.
(35) Doise, J.; Bekaert, J.; Chan, B. T.; Gronheid, R.; Cao, Y.; Hong, S.; Lin, G.; Fishman, D.; Chakk, Y.; Marzook, T. Implementation of surface energy modification in graphoepitaxy directed self-assembly for hole multiplication. *J. Vac. Sci. Technol., B: Nanotechnol. Microelectron.: Mater., Process., Meas., Phenom.* **2015**, *33*, 06F301.
(36) Li, W.; Nealey, P. F.; De Pablo, J. J.; Müller, M. Defect removal in the course of directed self-assembly is facilitated in the vicinity of the order-disorder transition. *Phys. Rev. Lett.* **2014**, *113*, 1−5.
(37) Hur, S.-M.; Thapar, V.; Ramírez-Hernández, A.; Khaira, G.; Segal-Peretz, T.; Delgadillo, P. A. R.; Li, W.; Müller, M.; Nealey, P. F.; de Pablo, J. J. Molecular pathways for defect annihilation in directed self-assembly. *Proc. Natl. Acad. Sci. U. S. A.* **2015**, *112*, 14144−14149.
(38) Laachi, N.; Iwama, T.; Delaney, K. T.; Shykind, D.; Weinheimer, C. J.; Fredrickson, G. H. Directed self-assembly of linear arrays of block copolymer cylinders. *J. Polym. Sci., Part B: Polym. Phys.* **2015**, *53*, 317−326.
(39) Li, W.; Müller, M. Thermodynamics and Kinetics of Defect Motion and Annihilation in the Self-Assembly of Lamellar Diblock Copolymers. *Macromolecules* **2016**, *49*, 6126−6138.
(40) Matsen, M. W.; Schick, M. Stable and Unstable Phases of a Linear Multiblock Copolymer Melt. *Macromolecules* **1994**, *27*, 7157−7163.
(41) Fredrickson, G. *The Equilibrium Theory of Inhomogeneous Polymers*; Oxford University Press: 2005; pp 1−456.
(42) Detcheverry, F. A.; Pike, D. Q.; Nealey, P. F.; Muller, M.; de Pablo, J. J. Monte Carlo Simulation of Coarse Grain Polymeric Systems. *Phys. Rev. Lett.* **2009**, *102*, 197801.
(43) Detcheverry, F. A.; Kang, H.; Daoulas, K. C.; Müller, M.; Nealey, P. F.; de Pablo, J. J. Monte Carlo Simulations of a Coarse Grain Model for Block Copolymers and Nanocomposites. *Macromolecules* **2008**, *41*, 4989−5001.
(44) Detcheverry, F. A.; Liu, G.; Nealey, P. F.; de Pablo, J. J. Interpolation in the Directed Assembly of Block Copolymers on Nanopatterned Substrates: Simulation and Experiments. *Macromolecules* **2010**, *43*, 3446−3454.
(45) E, W.; Ren, W.; Vanden-Eijnden, E. String method for the study of rare events. *Phys. Rev. B: Condens. Matter Mater. Phys.* **2002**, *66*, 052301.
(46) E, W.; Ren, W.; Vanden-Eijnden, E. Simplified and improved string method for computing the minimum energy paths in barrier-crossing events. *J. Chem. Phys.* **2007**, *126*, 164103.
(47) E, W.; Ren, W.; Vanden-Eijnden, E. Finite Temperature String Method for the Study of Rare Events. *J. Phys. Chem. B* **2005**, *109*, 6688−6693.
(48) Vanden-Eijnden, E.; Venturoli, M. Revisiting the finite temperature string method for the calculation of reaction tubes and free energies. *J. Chem. Phys.* **2009**, *130*, 194103.
(49) Maragliano, L.; Fischer, A.; Vanden-Eijnden, E.; Ciccotti, G. String method in collective variables: Minimum free energy paths and isocommittor surfaces. *J. Chem. Phys.* **2006**, *125*, 024106.
(50) Maragliano, L.; Vanden-Eijnden, E. On-the-fly string method for minimum free energy paths calculation. *Chem. Phys. Lett.* **2007**, *446*, 182−190.
(51) Miller, T. F.; Vanden-Eijnden, E.; Chandler, D. Solvent coarse-graining and the string method applied to the hydrophobic collapse of a hydrated chain. *Proc. Natl. Acad. Sci. U. S. A.* **2007**, *104*, 14559−14564.
(52) Cheng, X.; Lin, L.; E, W.; Zhang, P.; Shi, A.-C. Nucleation of Ordered Phases in Block Copolymers. *Phys. Rev. Lett.* **2010**, *104*, 148301.
(53) Ting, C. L.; Appelö, D.; Wang, Z.-G. Minimum Energy Path to Membrane Pore Formation and Rupture. *Phys. Rev. Lett.* **2011**, *106*, 168101.

DOI: 10.1021/acs.macromol.7b02639
Macromolecules XXXX, XXX, XXX−XXX

(54) Müller, M.; Smirnova, Y. G.; Marelli, G.; Fuhrmans, M.; Shi, A.-C. Transition Path from Two Apposed Membranes to a Stalk Obtained by a Combination of Particle Simulations and String Method. *Phys. Rev. Lett.* **2012**, *108*, 228103.

DOI: 10.1021/acs.macromol.7b02639
Macromolecules XXXX, XXX, XXX−XXX